



Ultra-low thermal conductivity of orthorhombic $\text{CH}_3\text{NH}_3\text{SnI}_3$: A first principles investigation



Vineet Kumar Sharma^a, V. Kanchana^{a,*}, Mayanak K. Gupta^b, Ranjan Mittal^{b,c}

^a Department of Physics, Indian Institute of Technology Hyderabad, Kandi, 502285, Sangareddy, Telangana, India

^b Solid State Physics Division, Bhabha Atomic Research Centre Trombay, Mumbai, 400085, India

^c Homi Bhabha National Institute, Anushaktinagar, Mumbai, 400094, India

ARTICLE INFO

Keywords:

Electronic structure
Phonon lifetime
Thermal conductivity

ABSTRACT

Here, we report the first principles studies of the mechanical, dynamical, electronic and thermal conductivity in the orthorhombic phase of $\text{CH}_3\text{NH}_3\text{SnI}_3$, which belong to perovskite family. The mechanical and dynamical properties ensure the stability of the investigated system. The electronic structure properties reveal the semi-conducting nature with narrow band gap of 0.5 eV. The detailed analysis of other phonon based properties like phonon lifetime, mean free path along with phonon spectrum reveal the enhanced phonon-phonon interactions, which are responsible for ultra low value of lattice thermal conductivity, which is the main highlights of the present work.

1. Introduction

Perovskite halides (ABX_3) of group 14 elements like Ge, Sn and Pb have been studied vastly because of the presence of phase transformation and diversity in electrical properties like ferroelectricity, ionic and electronic conductivity. The main attractive part of such materials are the presence of low oxidation state elements with a lone pair of s-electron [1–8]. These are responsible for their attractive structural and electrical properties. Another frontier part of this material's attraction is possessing the organic-inorganic framework which has drawn a great attention of researchers because of their low cost and cheaper processing techniques [9–11]. Lots of studies on $\text{CH}_3\text{NH}_3\text{PbI}_3$ have been reported because of its solar cell efficiency being better than silicon solar cells. These studies report that the power conversion efficiency of this compound has been enhanced from 3.8% [12] to 22.1% [13]. These Pb-based perovskites, $\text{CH}_3\text{NH}_3\text{PbX}_3$ ($X = \text{Cl}, \text{Br}, \text{I}$) have been reported as highly efficient solar cell materials as well as good thermoelectrics with high Seebeck coefficients [14–19]. Since, this material possesses high Seebeck coefficients [20], it might be applicable in solar thermoelectric generators [21], utilizing sunlight and converting it into electricity in terms of Seebeck effect [22,23].

Although these materials possess the highly efficient applications, they are Pb-based materials which are toxic in nature. This toxic nature is not fruitful for wide applications and finding another material to replace

lead based perovskite with such applications was a difficult task. A lot of research has been done in the past years in search of good alternative for $\text{CH}_3\text{NH}_3\text{PbX}_3$ ($X = \text{Cl}, \text{Br}, \text{I}$). In that approach, two other perovskites $\text{CH}_3\text{NH}_3\text{SnX}_3$ and $\text{CH}_3\text{NH}_3\text{GeX}_3$ where, ($X = \text{Cl}, \text{Br}$ and I) have been found which are good for solar cell applications in addition to being environment friendly [24–27]. These Pb free perovskites have been explored for their electrical, photo-responsive properties and for device simulation with high efficiency. First principles study of electronic structure and charge carrier mobility of $\text{CH}_3\text{NH}_3\text{SnI}_3$ has been explored by Li-Juan Wu and his group. They reported that this material could be a solar cell absorber and p-type semiconductor because of huge anisotropy in hole and electron mobilities [26]. Other studies on $\text{CH}_3\text{NH}_3\text{SnI}_3$ by Feng et al. reported that the band gap engineering under the low hydrostatic pressure is a good tool to match visible light spectrum [28]. In the recent work, the second order non-linear optical properties on inorganic-organic perovskites has been explored, and further adds more flavour to the utility of these halide based perovskites for their the optical applications [29]. In addition to that, the optical properties of $\text{CH}_3\text{NH}_3\text{SnI}_3$ are reported in triclinic phase, which is a low-temperature phase. This study opens the channel of utilizing a single source in its different structural phase.

Large Seebeck coefficients and possible solar thermoelectric applications serve as motivation for further computational studies on $\text{CH}_3\text{NH}_3\text{SnI}_3$ [30–33]. $\text{CH}_3\text{NH}_3\text{SnI}_3$ has been reported in different

* Corresponding author.

E-mail address: kanchana@iith.ac.in (V. Kanchana).

<https://doi.org/10.1016/j.jssc.2020.121541>

Received 14 April 2020; Received in revised form 28 May 2020; Accepted 22 June 2020

Available online 15 July 2020

0022-4596/© 2020 Elsevier Inc. All rights reserved.

Table 1Optimized parameters using different schemes of $\text{CH}_3\text{NH}_3\text{SnI}_3$ compared with earlier reported parameters by Feng et al.

| Parameters/Methods | Feng et al. work [28] | Becke 05 [47] | DFT - D2 [48] | DFT - D3 [49] | MK [50] | OR [50] | RE [51] | PBE [52] | LDA [53] |
|--------------------|-----------------------|---------------|---------------|---------------|---------|---------|---------|----------|----------|
| a () | 8.55 | 8.43 | 8.50 | 8.49 | 8.39 | 8.52 | 8.67 | 8.50 | 8.16 |
| b () | 12.42 | 12.61 | 12.71 | 12.72 | 12.52 | 12.72 | 12.94 | 12.70 | 12.26 |
| c () | 8.32 | 8.97 | 9.19 | 9.19 | 8.93 | 9.09 | 9.25 | 9.19 | 8.75 |
| Volume () | 885.34 | 953.43 | 993.13 | 993.03 | 940.59 | 985.76 | 1038.67 | 993.19 | 876.52 |

structural phases as a function of temperature in earlier studies [13, 34–38]. Rahul Singh et al. [40] studied the transport properties like thermopower etc. of $\text{CH}_3\text{NH}_3\text{PbI}_3$ and $\text{CH}_3\text{NH}_3\text{SnI}_3$ in their cubic phase and band gap engineering were also reported using superlattice approach. Thermopower of $\text{CH}_3\text{NH}_3\text{SnI}_3$ reported in orthorhombic, tetragonal and cubic phases in another previous work, and found the thermopower positive which was evident to claim that the thermopower is due to holes only [41]. The previous studies on $\text{CH}_3\text{NH}_3\text{SnI}_3$ confirm that the lattice thermal conductivity of $\text{CH}_3\text{NH}_3\text{SnI}_3$ is not reported till now both experimentally as well as theoretically in any structural phase. The thermal conductivity is a key parameter in deciding the dimensionless figure of merit ZT, which characterise the efficiency of any thermoelectric material.

$$ZT = \frac{S^2 \sigma}{\kappa} \quad (1)$$

where, κ is sum of the electronic part of thermal conductivity κ_e and lattice thermal conductivity κ_l . Its value must be low for good thermoelectric material. One should choose a material with low lattice thermal conductivity for better thermoelectric performance as can be seen from the above relation. This justifies the importance of the present work. The earlier studies on $\text{CH}_3\text{NH}_3\text{PbX}_3$ reported it as good thermoelectric material and possess ultra-low value of lattice thermal conductivity [42], which serve as a reference for opting this lead free system. The present work is organised as follows. Firstly, the methodology has been discussed in section 2. Section 3 reports the results and discussions and finally, conclusions are given in section 4.

2. Computational methods

Full geometry optimization has been carried out using pseudopotential method implemented in Vienna Ab-initio Simulation Package (VASP) [43–46] within the framework of density functional theory to get optimized parameters. We have chosen different functionals [47–53] to get optimized ground state of this system. We have used DFT-D2 [48] and DFT-D3 [49] methods to include vander Waal's correction to ground state energy. The energy convergence and force tolerance are set as 10^{-8} Ry and -10^{-2} eV/Å respectively. Out of all the chosen functionals, the

optimized parameters with LDA exchange correlation functional are in good accord with experimental parameters [28]. The special k-mesh in the Irreducible Brillouin Zone (IBZ) was $16 \times 16 \times 16$ according to Monkhorst-Pack scheme [54]. Tetrahedron method [55] was used to integrate the Brillouin zone. The plane wave cut-off energy is set to 900 eV to get good converged ground state properties. The elastic tensor calculations has been done using second order derivative of forces generated through VASP.

The phonon dispersion calculations has been performed using combination of VASP and Phonopy [56] with frozen phonon technique. We have computed the electronic structure properties using optimized ground state eigenvalues. Next, the Boltzmann theory has been employed on our converged calculations as implemented in BoltzTraP code [57], within the constant scattering time approximation (CSTA) and rigid band approximation (RBA) [58–60] to calculate the electrical conductivity scaled by relaxation time. The lattice thermal conductivity κ_l of the investigated compound is being calculated using force constant method within relaxation time approximation in combination with phono3py [61] and VASP. Second and third-order force constants were obtained through supercell approach with finite displacements of 0.03 Å.

3. Results and discussions

3.1. Structural and electronic structure properties

$\text{CH}_3\text{NH}_3\text{SnX}_3$ (X = Br and I) exist in different phases as a function of temperature similar to $\text{CH}_3\text{NH}_3\text{PbX}_3$ and undergoes structural transition from cubic, tetragonal, orthorhombic and monoclinic phases to triclinic phase on lowering the temperature [13,34–38]. The disordering of $(\text{CH}_3\text{NH}_3)^+$ and the distortions of $(\text{SnX}_3)^-$ octahedra at finite temperature are the cause of such complicated phase transitions in $\text{CH}_3\text{NH}_3\text{SnX}_3$ [13,34–37]. The orientation of $(\text{CH}_3\text{NH}_3)^+$ cations are completely disordered while the SnX_6 structural units possess cubic symmetry in high temperature cubic phase. As we reduce the temperature, the disordering of these cations suppresses due to tilting and distortion of SnX_6 octahedras. The low temperature phase show more ordered orientation of $(\text{CH}_3\text{NH}_3)^+$ cations. From the earlier reported work, it is found that the unit cell of monoclinic phase deviates very slightly from orthorhombic

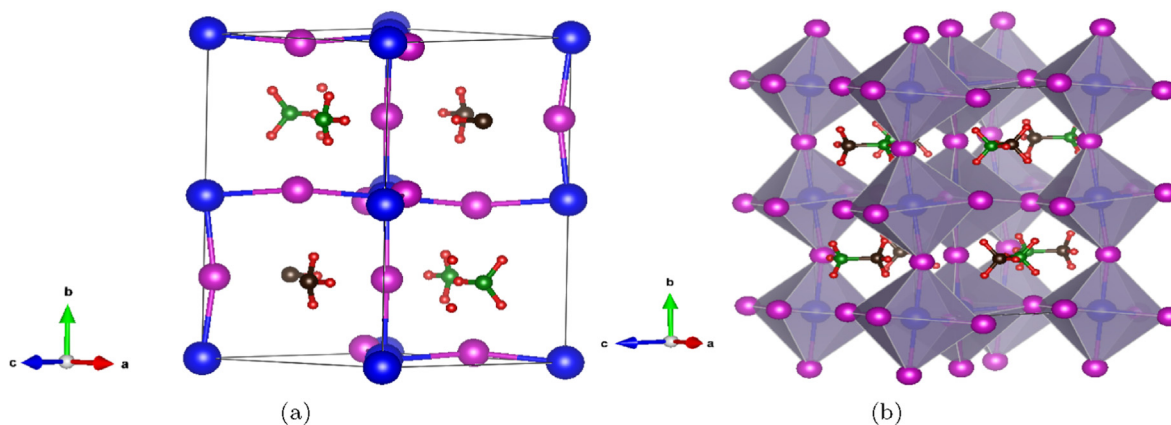


Fig. 1. Crystal structure of $\text{CH}_3\text{NH}_3\text{SnI}_3$. (a) The conventional unit cell and (b) Polyhedral view (Sn - Blue, I - Purple, N - Green, C - Brown and H - Red). (For interpretation of the references to color in this figure legend, the reader is referred to the Web version of this article.)

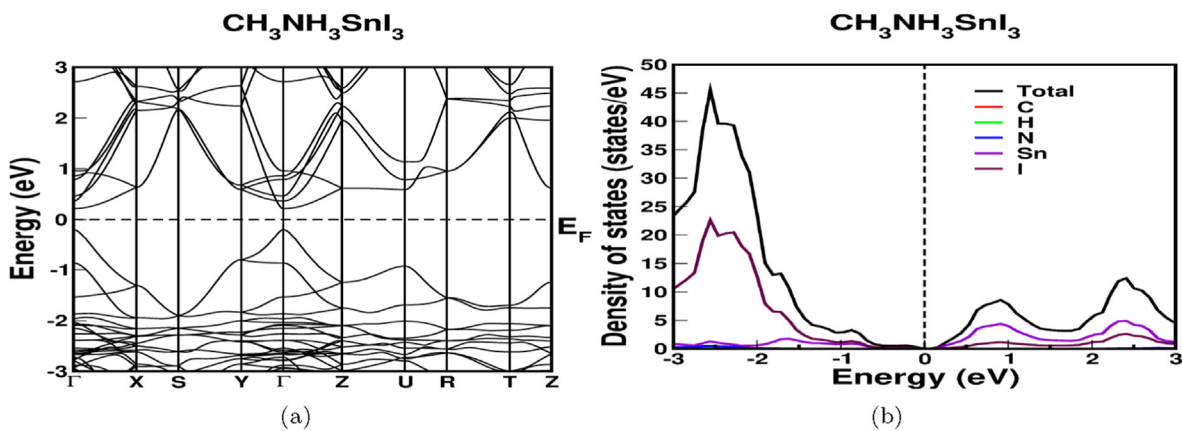


Fig. 2. Electronic structure properties of $\text{CH}_3\text{NH}_3\text{SnI}_3$, (a) band structure and (b) Total Density of states and projected density of states.

phase which is another low temperature phase [38,39]. So, one can take orthorhombic unit cell to approximate the real structure.

The low-temperature orthorhombic phase of $\text{CH}_3\text{NH}_3\text{SnI}_3$ with space group Pnma (62) has been chosen for present study as reported earlier by Feng et al. [28]. Different exchange-correlation functionals have been used for geometry optimization. The optimized parameters using different schemes along with reported by Feng et. work are given in Table 1. Out of all exchange-correlation functionals LDA gives better results with least volume change. The crystal structure is shown in Fig. 1. Well converged optimized values have been taken as inputs for further investigation. Self-consistent calculations have been done to get the energy eigenvalues. The electronic structure properties have been calculated using the same eigenvalues and are given in Fig. 2. From the band plots, it is found that this system is a direct band gap semiconductor with narrow band gap of nearly 0.5 eV at Γ -point. The band plot is given in Fig. 2(a). In the earlier work [62], Li-Juan Wu et al. reported the electronic properties of $\text{CH}_3\text{NH}_3\text{SnI}_3$ using other exchange-correlation functional like DFT-D2 and HSE-06. The reported band gaps are 0.74 eV and 1.27 eV respectively [62]. The detailed analysis of band plots suggest that the bands are highly dispersive in valence band region compared to that lying in conduction band. The band dispersion plays a very important role in quantifying the thermoelectric properties of a material, because this dispersion is related to the effective mass of the charge carriers. The effective mass is inversely proportional to the curvature of bands which is nothing but second order derivative of band dispersion. In the present work, the bands are less dispersive in conduction band which results into higher value of thermopower for electrons than that of holes in valence band. The higher dispersivity of bands present in valence band region shows the possibility of high value of the electrical conductivity for holes.

The information of the states lying near Fermi level in both valence and conduction band can be obtained through the projected density of states and we have calculated total density of states along with projected density of states which are given in Fig. 2(b). The density of states also reflects the semiconducting nature as reported in band dispersion. Sn and I atoms are dominating near Fermi level in both band regions. The projected density of states analysis shows that Sn-s and I-p states are dominating in valence band near Fermi level, while Sn-p states are lying in conduction band near Fermi level. We can connect this orbital occupancy to band dispersion. The trend of band profile closest to Fermi level in valence band is parabolic which matches with s-orbital character.

3.2. Mechanical properties

The elastic constants have been calculated through second order derivative of energy per unit area using VASP and as a result nine independent elastic constants are generated through elastic tensor analysis for the orthorhombic symmetry of the system. The minimum criteria for stability of the system is that the elastic constants are positive which is

Table 2

Elastic properties of $\text{CH}_3\text{NH}_3\text{SnI}_3$.

| Compound/Elastic properties | Present work |
|-----------------------------|--------------|
| C_{11} (GPa) | 35.83 |
| C_{12} (GPa) | 13.54 |
| C_{13} (GPa) | 17.13 |
| C_{22} (GPa) | 44.88 |
| C_{23} (GPa) | 14.12 |
| C_{33} (GPa) | 28.73 |
| C_{44} (GPa) | 5.85 |
| C_{55} (GPa) | 15.72 |
| C_{66} (GPa) | 5.03 |
| Bulk Modulus (GPa) | 21.89 |
| Shear Modulus (GPa) | 8.71 |
| Young's modulus (GPa) | 23.07 |
| Poisson's ratio(ν) | 0.32 |
| ρ (gm/cc) | 4.03 |
| v_l (Km/s) | 2.88 |
| v_t (Km/s) | 1.47 |
| v_m (Km/s) | 1.64 |
| θ_D (K) | 186.34 |

not the necessary and sufficient condition. The Born's mechanical stability criteria is to be fulfilled to confirm its mechanical stability and the same for orthorhombic system is given as,

$$C_{11} > 0; C_{11}C_{22} > C_{12}^2$$

$$C_{11}C_{22}C_{33} + 2C_{12}C_{13}C_{23} - C_{11}C_{23}^2 - C_{22}C_{13}^2 - C_{33}C_{12}^2 > 0$$

$$C_{44} > 0; C_{55} > 0; C_{66} > 0$$

Using these elastic constants, we have computed other mechanical properties under Voigt [63] and Reuss [64] and Voigt-Reuss-Hill [65] approximations using following relations.

$$B_V = \frac{1}{9}[C_{11} + C_{22} + C_{33}] + \frac{2}{9}[C_{12} + C_{13} + C_{23}] \quad (2)$$

$$G_V = \frac{1}{15}[C_{11} + C_{22} + C_{33} - C_{12} - C_{13} - C_{23}] + \frac{3}{5}[C_{44} + C_{55} + C_{66}] \quad (3)$$

$$B_R = \frac{1}{[A + 2B]} \quad (4)$$

$$G_R = \frac{15}{[4A - B + 3C]} \quad (5)$$

where, $A = s_{11} + s_{22} + s_{33}$, $B = s_{12} + s_{13} + s_{23}$ and $C = s_{44} + s_{55} + s_{66}$. s_{ij} are the inversion of the elastic constant matrix. According to Hill

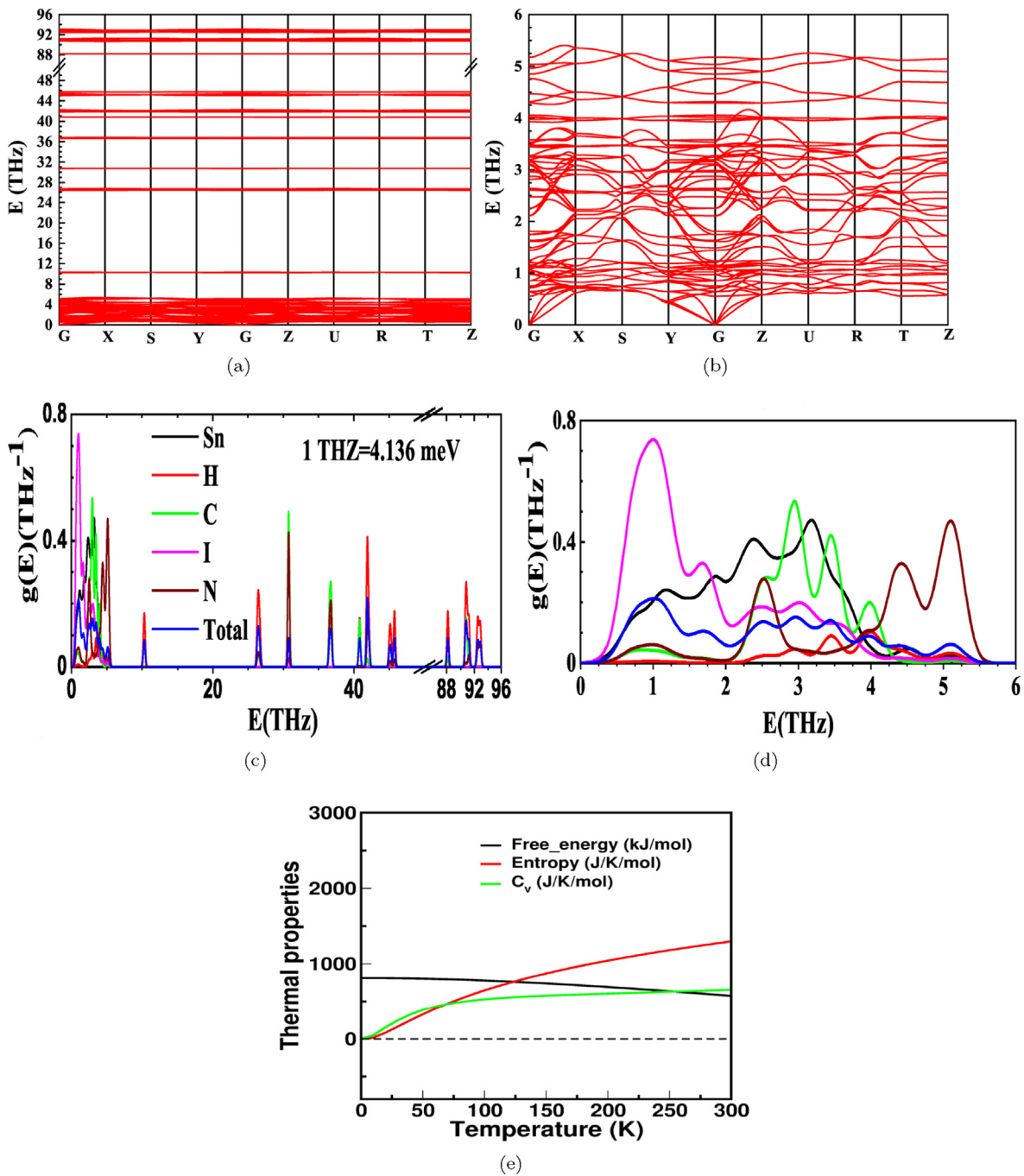


Fig. 3. The phonon dispersion in full range (a) and low frequency range (b), The phonon density of states in full range (c) and low frequency range (d), and (e) Thermal Properties.

approximation, the mechanical properties can be calculated using the following relations.

$$B_H = \frac{1}{2}(B_R + B_V); G_H = \frac{1}{2}(G_R + G_V) \quad (6)$$

$$E_H = \frac{9B_H G_H}{3B_H + G_H}; \nu = \frac{(3B_H - 2G_H)}{2(B_H + G_H)} \quad (7)$$

All the calculated mechanical properties are given in Table 2. These mechanical properties play a major role to convey the information about the resistance to fracture and their mechanical strength. How much strain, a system can bear before breaking? This can be understood from

the elasticity of the system. Elasticity depends on Young's modulus. Higher the Young's modulus, higher the elasticity. The shear modulus shows the resistance to fracture of the material. The value of bulk modulus is related to compressibility of the material. Poisson's ratio is very important property of a material because its value decides the ductile and brittle nature of the materials. If the value of Poisson's ratio is more than 0.17, it implies that the investigated system is ductile in nature. We have done comparative analysis of mechanical properties with earlier reported work. Ali et al. [66] analysed the mechanical properties under 0.7 GPa, while J. Feng [67] reported at ambient using GGA-PBE functional. We have calculated mechanical properties using LDA functional and our values can be compared with ambient results reported by Feng et al. The calculated mechanical properties are in good

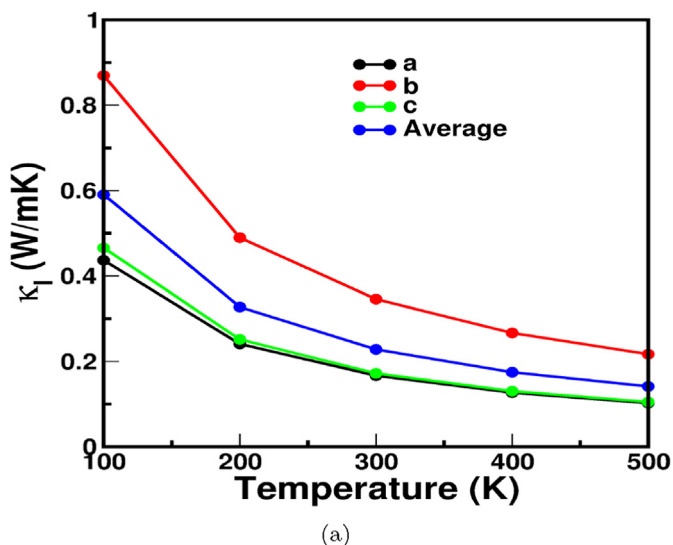


Fig. 4. Thermal conductivity of $\text{CH}_3\text{NH}_3\text{SnI}_3$.

accord with the value reported by Feng et al. except for few minor differences. These differences are due to the exchange-correlation functional being different.

We have calculated Debye temperature which is very important parameter for any material, and not reported in any previous studies done so far for the investigated compound. The importance of Debye temperature θ_D is that it is highly connected to the lattice thermal con-

ductivity of the system. The Debye temperature θ_D is the temperature which corresponds to crystal's highest normal mode of vibration which connects the elastic properties to the thermodynamic and thermal properties such as phonons, thermal expansion, thermal conductivity, specific heat, and lattice enthalpy [68]. In general, the Debye temperature of most crystals are lying between 200 K–400 K [69]. The value of Debye temperature affects the thermal conductivity of the materials. Higher the value of θ_D , higher would be the κ_l . In the present work, the reported value of Debye temperature is very low which means that the lower value of κ_l could be expected in the investigated compound which has been verified in the present work.

3.3. Dynamical properties

The phonon dispersion has been calculated to check dynamical stability of the investigated compound at ambient. The phonon dispersion plots are given in Fig. 3(a and b). The phonon dispersion has been plotted in full range up to 96 THz [Fig. 3(a)]. The low frequency range is displayed in Fig. 3(b). The absence of negative frequencies in phonon dispersion ensures its stability which can be seen from Fig. 3(a). From the phonon dispersion, we found that the optical modes lying in low frequency region are highly interacting. These interactions would be responsible for phonon scattering. The contribution to these phonon modes arises mainly from Sn and I ions. These ions are almost equal in atomic weights and this is responsible for highly interactive optical modes. There is a gap arising between the low frequency and the high frequency optical modes and this gap is due to huge difference in atomic weights between ions and it can be seen in Fig. 3(a). The high frequency optical modes are dominated by C, H and N ions which are very lighter than Sn and I ions. We have done the comparative analysis of the phonon

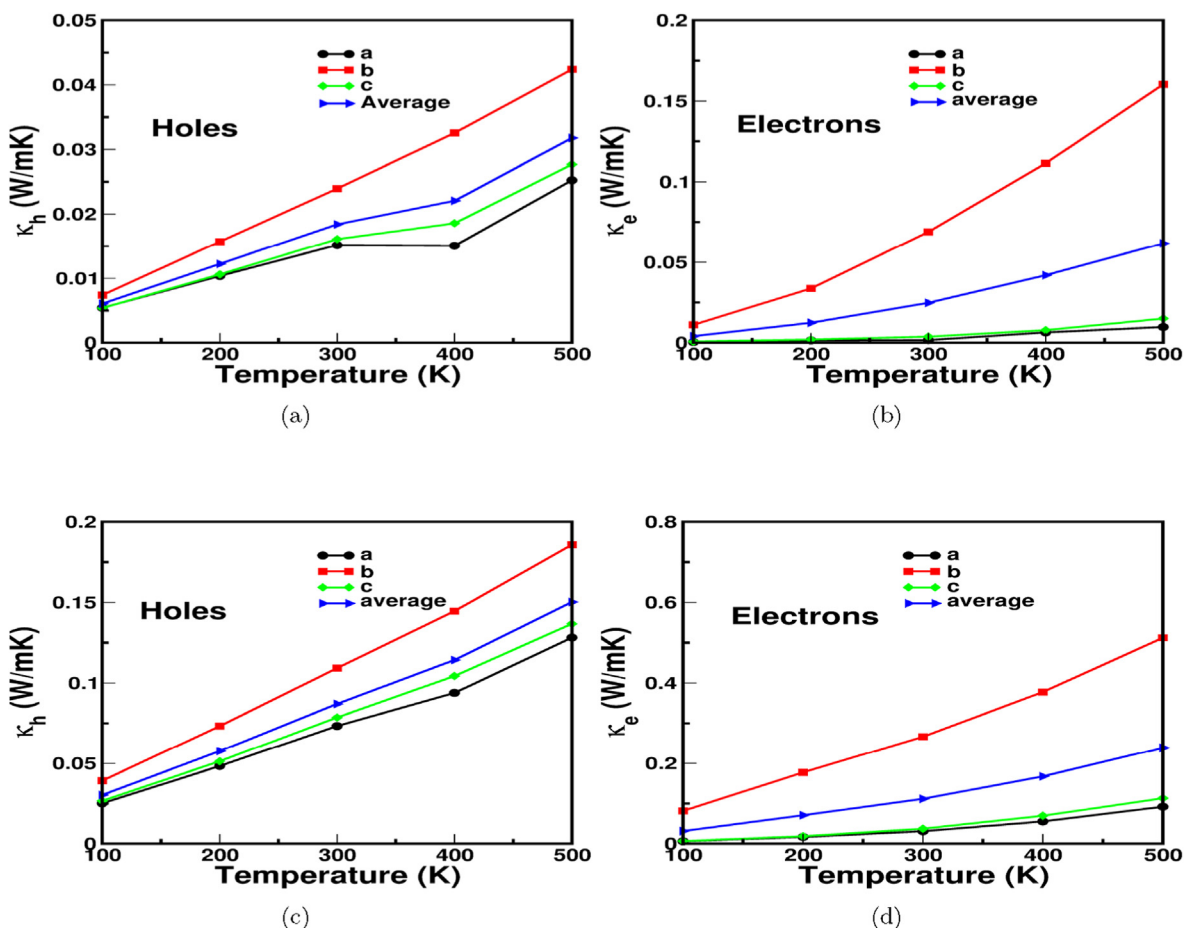


Fig. 5. (a, b) Electronic part of thermal conductivity of $\text{CH}_3\text{NH}_3\text{SnI}_3$ at 10^{19}cm^{-3} and (c, d) at 10^{20}cm^{-3} .

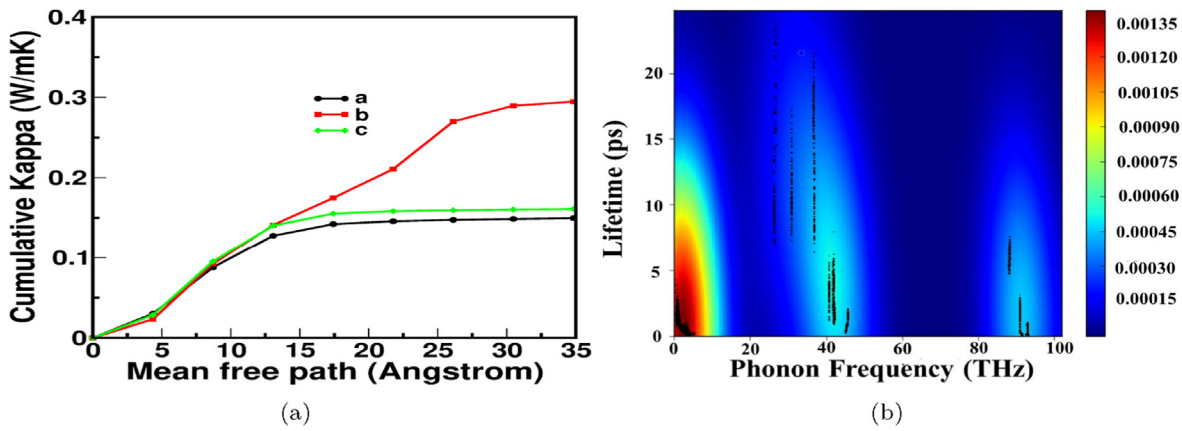


Fig. 6. (a) The cumulative lattice thermal conductivity κ_l as a function of mean free path of $\text{CH}_3\text{NH}_3\text{SnI}_3$ and (b) Phonon lifetime as a function of phonon frequency of $\text{CH}_3\text{NH}_3\text{SnI}_3$.

Table 3

Comparative study of thermoelectric properties at 300 K (Here, 'a', 'b' and 'c' correspond to crystallographic directions 'x', 'y' and 'z' respectively).

| Material | κ (W/mK) |
|--------------------------------------|-------------------------|
| SnSe | 0.46(a),0.7(b),0.68(c) |
| Sns | 1.25 |
| PbTe | 1.7 |
| $\text{CH}_3\text{NH}_3\text{SnI}_3$ | 0.17(a),0.35(b),0.17(c) |

dispersion of present study with earlier reported work [66]. The earlier study reports that the dynamical properties of $\text{CH}_3\text{NH}_3\text{SnI}_3$ are unstable at ambient condition, while stable at 0.7GPa using GGA-PBE functional. In the present work, the phonons are positive at ambient itself using LDA exchange-correlation functional. The total phonon density of states along with partial phonon density of states calculated as a function of phonon frequencies are given in Fig. 3(c) and (d). The phonon gap observed in phonon dispersion can be seen from phonon density of states plotted in full range [Fig. 3(c)]. The detailed analysis of phonon density of states infer that Sn and I atoms are dominating in low-frequency region while lighter entities like C, H and N are in high frequency region.

To correlate low frequency highly interacting modes observed in phonon dispersion, the phonon density of states are also plotted till 6 THz [Fig. 3(d)]. From Fig. 3(c and d), it is found that the contribution of Sn and I atoms to the total density of states in low frequency region is more and higher than the total density of states. The reason behind this contribution is that the atomic partial phonon density of states is

normalized to unity and the total phonon density of states is sum of weighted average of individual atoms. It infers that the lighter atoms are dominating up to full range while Sn and I are lying in lower range. Apart from the phonon dispersion, we have calculated other thermal properties like Helmholtz free energy, entropy and specific heat to show the thermodynamic stability and are given in Fig. 3(e). These properties have been calculated at constant volume using phonon density of states as a function of frequencies. The free energy is found to decrease gradually as a function of temperature and becomes negative. This behavior in free energy is normal under any natural process. The entropy of the system is increasing as function of temperature due to thermal agitation. The thermal agitation adds the disorder which enhances the entropy of the system. How does a material behave under different thermodynamic constraints? It can be understood through the specific heat which signifies the heat capacity of any system. From Fig. 3(e), we found that C_v is increasing sharply in low temperature region and finally approaching to a saturation point and beyond that it remains constant. This kind of nature of specific heat is very well-known in solids.

3.4. Thermal conductivity

The lattice thermal conductivity κ_l can be calculated using following empirical relation through phono3py [70],

$$\kappa_l = \frac{1}{NV_0} \sum_{\lambda} C_{\lambda} v_{\lambda} \otimes v_{\lambda} \tau_{\lambda} \quad (8)$$

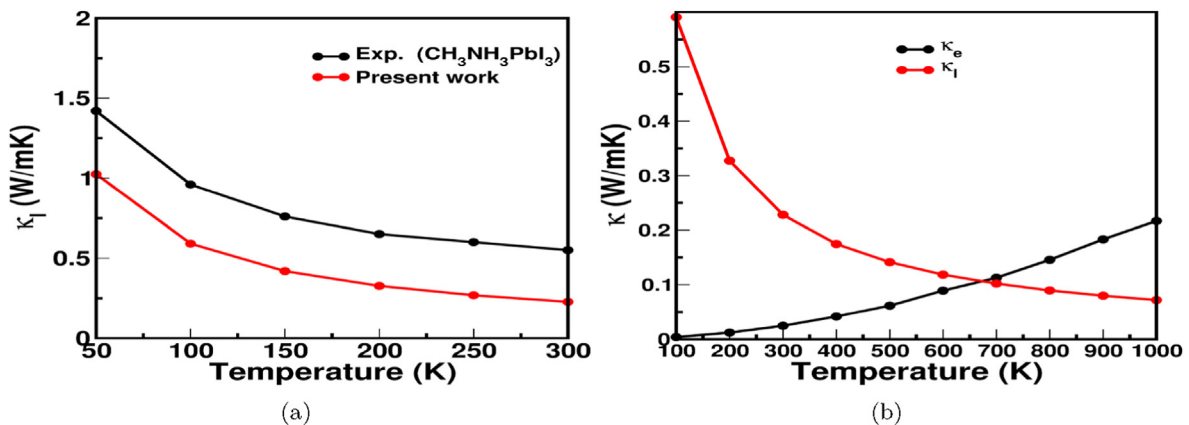


Fig. 7. (a)The comparative study of the lattice thermal conductivity with experimental results of the prototype compounds and (b) The variation of κ_l along with κ_e calculated for electron concentration 10^{19} cm^{-3} as a function of temperature.

where, N and V_0 are the number of unit cells in the system and volume of the unit cell, respectively. C_i is phonon mode heat capacity. v_i is group velocity. The third order force displacements has been generated with supercell size of $2 \times 1 \times 2$ using Phono3py and as a result, 10843 third order displacements along with 46 s order force displacements have been generated. The K-mesh sampling of $4 \times 2 \times 4$ and $2 \times 2 \times 2$ in reciprocal space has been used for third order and second order forces respectively. Computing this large no. of data is computationally expensive. The mesh-sampling of $5 \times 5 \times 5$ has been used to compute converged κ_l . This is a key parameter in the area of thermoelectrics which must be low for feasible thermoelectric applications. The lattice thermal conductivity is given by Fig. 4. Here, the lattice thermal conductivity along the three crystallographic directions has been calculated to see the possibility of anisotropic behavior. From the plots, the lattice thermal conductivity is found to have anisotropy. The anisotropic factor between 'a' and 'c' axes is found to decrease with temperature. Thermal conductivity κ_l along 'b' axis is higher than remaining two axes. The lattice part of thermal conductivity is characterized through lattice information which is connected to phonons. This anisotropy is due to the phonon-phonon interactions being different along different crystallographic axes as displayed in Fig. 3(b). From the low frequency phonon dispersion, it can be seen that the phonon dispersion along 'a' and 'c' axes are almost similar and softer than that along 'b' axis. The group velocity is a slope of both the acoustic and optical phonon modes. As dispersion differs along 'b' axis than that along remaining two axes, same effect will be reflected in group velocities too. The anisotropic nature in group velocities along with phonon dispersion are responsible for anisotropic nature of the lattice thermal conductivity. One earlier study on Td-WTe₂ [71] also report the same. The average thermal conductivity is being calculated using relation $(\kappa_a + \kappa_b + \kappa_c)/3$ and is given in Fig. 4. The minimal thermal conductivity has been calculated using Cahill's model [72] to correlate analytical results with computational approach. The minimal thermal conductivity is 1.15 W/mK.

The electronic part of thermal conductivity has been calculated using Wiedman Frenz law given by following formula,

$$\kappa_e = L\sigma T \quad (9)$$

where, L is Lorentz number ($L = 2.45 \times 10^{-8} \text{ W}\Omega/\text{K}^2$). The calculated electrical conductivity scaled by relaxation time has been taken into account to compute κ_e . Here, we have assumed the relaxation time τ as 10^{-15} s for getting σ alone. The electronic thermal conductivity at different carrier concentration are given in Fig. 5. From the plots, we have observed the lattice thermal conductivity dominating below room temperature, while the electronic thermal conductivity is more pronounced above room temperature as expected. An anisotropy in κ_e has been found specially, in case of electrons similar to κ_l . Fig. 6(a) displays the cumulative lattice thermal conductivity as a function of phonon mean free path. From the figure, it is found that the κ_l along 'a' and 'c' axis is mainly dominated by the phonons whose mean free path (MFP) are lesser than 13. On the other hand, κ_l along 'b' axis is dominated by the phonons with MFP lower than 30.

Next, we have computed phonon lifetime as a function of phonon frequency which is given in Fig. 6(b). The color bar values depict the density of phonon modes. These density of phonon modes infer that the low frequency phonon modes are having shorter lifetime ranging from 0 to 13 ps? In the low frequency region, we could see that there is a considerable interaction between the acoustic and the optical phonon modes, which would certainly result in larger phonon scattering [73], which would eventually reduce the phonon mean free path. The lattice thermal conductivity is also linked to the mean free path through the relation [74],

$$\kappa_{accum} = \sum_s \int_0^{l^*} \frac{1}{3} C_{MFP}(l) v(l) |dl| \quad (10)$$

where, l is the phonon MFP, v is the phonon group velocity, C_{MFP} is the volumetric heat capacity per unit phonon MFP, and s indexes the polarization of phonons. Since the integral is taken from 0 to l^* , κ_{accum} quantifies the contribution to bulk thermal conductivity of phonons with a MFP less than or equal to l^* . Here as the system is anisotropic, we need to use the mean free path along the respective direction. The cumulative thermal conductivity as a function of mean free path displays that major contribution is arising from the shorter mean free path. This scattering is the main cause of low lattice thermal conductivity in the investigated system. We have compared our values of the lattice thermal conductivity with earlier reported work on lead based halide perovskite $\text{CH}_3\text{NH}_3\text{PbI}_3$ [66], as there is no earlier experimental study available for the present compound. From the comparative analysis, we conclude that our values are in good accord with earlier work in low temperature range. Thermal conductivity of the investigated organic compound is very low and in good accord with other studies on thermoelectrics with low thermal conductivity [75–77] (see Table 3). Next, we have plotted the experimental data of κ_l reported for $\text{CH}_3\text{NH}_3\text{PbI}_3$ [42] along with lattice thermal conductivity of $\text{CH}_3\text{NH}_3\text{SnI}_3$ ranging from 50 K to 300 K [Fig. 7(a)]. Here, this comparative analysis has been done for two reasons, one is to match up the trend of the calculated κ_l with experimentally reported for prototype compound and other is to see the variation in κ_l from Sn to Pb. The comparative analysis suggests that $\text{CH}_3\text{NH}_3\text{SnI}_3$ has lower κ_l with difference of 0.4 W/mK than $\text{CH}_3\text{NH}_3\text{PbI}_3$. Fig. 7(b) displays both the electronic and lattice part of thermal conductivity. From the plots, it can be said that κ_l is dominating in low temperature region while κ_e in high temperature region. κ_e has been calculated for electron concentration around 10^{19} cm^{-3} .

4. Conclusion

First principles studies suggest that the investigated compound is mechanically, thermodynamically and dynamically stable. The electronic properties reveal that it is a direct band gap semiconductor. The lattice thermal conductivity has been calculated using third and second order force constants. The ultra-low value of the lattice thermal conductivity has been reported. The phonon lifetime shows the low frequency phonon-phonon interactions which results in lowering of lattice thermal conductivity. The anisotropy in the lattice thermal conductivity could be due to group velocities being different along different crystallographic axes. The present study reveals that $\text{CH}_3\text{NH}_3\text{SnI}_3$ possess very low thermal conductivity.

Declaration of competing interest

The authors declare that they have no known competing financial interests or personal relationships that could have appeared to influence the work reported in this paper.

CRediT authorship contribution statement

Vineet Kumar Sharma: Formal analysis, Writing - original draft. **V. Kanchana:** Formal analysis, Writing - original draft, Writing - review & editing. **Mayanak K. Gupta:** Writing - review & editing. **Ranjan Mittal:** Formal analysis, Writing - review & editing.

Acknowledgement

Both VKS and VK would like to acknowledge IIT Hyderabad for providing computational facilities. VKS would like to acknowledge MHRD for fellowship. The authors would like to acknowledge to BRNS project with sanction no.(58/14/13/2019-BRNS).

References

- [1] G. Thiele, H.W. Rotter, K.D. Schmidt, Z. Anorg. Chem. 148 (1987) 545.
- [2] G. Thiele, H.W. Rotter, K.D. Schmidt, Z. Anorg. Chem. 7 (1988) 559.
- [3] W. Depmeier, A. Möller, Acta Crystallogr. B 36 (1980) 803.
- [4] K. Yamada, S. Nose, T. Umehara, T. Okuda, S. Ichiba, Bull. Chem. Soc. Jpn. 61 (1988) 4265.
- [5] K. Yamada, S. Funabiki, H. Horimoto, T. Matsui, T. Okuda, S. Ichiba, Chem. Lett. 801 (1991).
- [6] S. Plesko, R. Kind, J. Roots, J. Phys. Soc. Jpn. 45 (1978) 553.
- [7] S. Sharma, N. Weiden, A. Weiss, Z. Natureforsch. Teil A 46 (1991) 329.
- [8] A. Poglitsch, D. Weber, J. Chem. Phys. 87 (1987) 63–73.
- [9] S. Kazim, M.K. Nazeemuddin, M. Gratzel, S. Ahmed, Angew. Chem. Int. Ed. 53 (2014) 2812.
- [10] B.V. Lotsch, Angew. Chem. Int. Ed. 53 (2014) 635.
- [11] Z.H. Wei, H.N. Chen, K.Y. Yan, S.H. Yang, Angew. Chem. Int. Ed. 53 (2014) 13239.
- [12] A. Kojima, K. Teshima, Y. Shirai, T. Miyasaka, J. Am. Chem. Soc. 131 (2009) 6050.
- [13] C.C. Stoumpos, C.D. Malliakas, M.G. Kanatzidis, Inorg. Chem. 52 (2013) 9019, 2009.
- [14] Noriko Onoda-Yamamuro, Takasuke Matsuo, Hiroshi Suga, J. Phys. Chem. Solid. 53 (7) (1992) 935–939.
- [15] Zhang, et al., ACS Nano 9 (4) (2015) 4533–4542.
- [16] Feng Jing, Bing Xiao, J. Phys. Chem. Lett. 5 (2014) 1278–1282.
- [17] Takumi Yamada, Yasuhiro Yamada, Yumi Nakaike, Atsushi Wakamiya, Yoshihiko Kanemitsu, Phys. Rev. Appl. 7 (2017), 014001.
- [18] Long Xiang, Zhenyu Pan, Zhuolei Zhang, Jeffrey J. Urban, Heng Wang, Appl. Phys. Lett. 115 (2019), 072104.
- [19] Ping Wu, Yan Xiong, Lin Sun, Xie Guo, Ling Xu, Org. Electron. 55 (2018) 90–96.
- [20] Y. Takahashi, H. Hasegawa, T. Inabe, J. Solid State Chem. 39 (2013) 205.
- [21] Y. He, G. Galli, Chem. Mater. 26 (2014) 5394.
- [22] D. Kraemer, B. Poudel, H.P. Feng, J.C. Caylor, B. Yu, X. Yan, Y. Ma, X. wang, D. Wang, A. Muto, K. McEnaney, M. Chiesa, Z. Ren, G. Chen, Nat. Mater. 10 (2011) 532.
- [23] L.L. Baranowski, G.J. Snyder, E.S. Toberer, Energy Environ. Sci. 5 (2012) 9055.
- [24] Y.Q. Huang, J. Su, Q.F. Li, D. Wang, L.H. Xu, Y. Bai, Phys. B Condens. Matter 563 (2019) 107–112.
- [25] Lü Xujie, et al., Adv. Mater. 28 (2016) 8663–8668.
- [26] Li-Juan Wu, Yu-Qing Zhao, Chang-Wen Chen, Lin-Zhi Wang, Biao liu and meng-qi cai, Chin. Phys. B 25 (10) (2016) 107202.
- [27] Hui-Jing Du, Wei-Chao Wang, Jian-Zhuo Zhu, Chin. Phys. B 25 (10) (2016) 108802.
- [28] J. Feng, B. Xiao, J. Phys. Chem. C 118 (2014) 19655.
- [29] Wenshen Song, Guang-Yu Guo, Su Huang, Lan Yang, Li Yang, Physical Review Applied 13 (2020), 014052.
- [30] C. Quarti, E. Mosconi, F. De Angelis, Phys. Chem. Chem. Phys. 17 (2015) 9394.
- [31] E. Mosconi, A. Amat, M.K. Nazeeruddin, M. Grätzel, F. De Angelis, J. Phys. Chem. C 117 (2013) 13902.
- [32] S. Colella, et al., Chem. Mater. 25 (2013) 4613.
- [33] F. Brivio, K.T. Butler, A. Walsh, M. van Schilfgarde, Phys. Rev. B 89 (2014) 155204.
- [34] N. Onoda-Yamamuro, T. Matsuo, H. Suga, J. Phys. Chem. Solid. 51 (12) (1990) 1383–1395.
- [35] H. Mashiyama, Y. Kurihara, T. Azetsu, J. Kor. Phys. Soc. 32S (1998) S156–S158.
- [36] Y. Kawamura, H. Mashiyama, K. Hasebe, J. Phys. Soc. Jpn. 71 (7) (2002) 1694–1697.
- [37] I. Borriello, G. Cantele, D. Ninno, Phys. Rev. B 77 (2008) 23521423.
- [38] F. Chiarella, A. Zappettini, F. Licci, I. Borriello, G. Cantele, D. Ninno, A. Cassinese, R. Vaglio, Phys. Rev. B 77 (2008), 0451294.
- [39] Y. Takahashi, R. Obara, Z.Z. Lin, Y. Takahashi, T. Naito, T. Inabe, S. Ishibashi, K. Terakura, Dalton Trans. 40 (20) (2011) 5563–5568.
- [40] Rahul Singh, Ranjith Kottokkaran, L. Vikram, Dalal and ganesh balasubramanian, Nanoscale 9 (2017) 8600–8607.
- [41] Yukari Takahashi, Hiroyuki Hasegawa, Yukihiko Takahashi, Tamotsu Inabe, J. Solid State Chem. 205 (2013) 39–43.
- [42] Andrea Pisoni, Jacim Jacimovic, Osar S. Barisic, Massimo Spina, Richard Gaal, Laszlo Forro, Endre Horvath, J. Phys. Chem. Lett. 5 (2014) 2488–2492.
- [43] G. Kresse, J. Hafner, Phys. Rev. B 47 (1993) 558.
- [44] G. Kresse, J. Furthmuller, Comput. Mater. Sci. 6 (1996) 15.
- [45] G. Kresse, J. Furthmuller, Phys. Rev. B 54 (1996) 11169.
- [46] G. Kresse, D. Joubert, Phys. Rev. 59 (1999) 1758.
- [47] A.D. Becke, J. Chem. Phys. 98 (1993) 5648–5652.
- [48] J. Harl, L. Schimka, G. Kresse, Assessing the quality of the random phase approximation for lattice constants and atomization energised of solids, Phys. Rev. B 81 (2010) 115126.
- [49] S. Grimme, J. Antony, S. Ehrlich, S. Krieg, A consistent and accurate ab-initio parametrization of density functional dispersion correction (dft-d) for the 94 elements H-Pu, J. Chem. Phys. 132 (2010) 154104.
- [50] J. Klimes, D.R. Bowler, A. Michaelides, J. Phys. Condens. Matter 22 (2010), 022201.
- [51] Y. Zhang, W. Yang, Phys. Rev. Lett. 80 (1998) 890.
- [52] J.P. Perdew, K. Burke, M. Ernzerhof, Phys. Rev. Lett. 77 (1996) 3865.
- [53] R.G. Parr, W. Yang, Density Functional Theory of Atoms and Molecules, Oxford University Press, New York, Oxford, 1989.
- [54] H.J. Monkhorst, J.D. Pack, Phys. Rev. B 13 (1976) 5188.
- [55] P. Blochl, O. Jepsen, O. Andersen, Phys. Rev. B 49 (1994) 16223.
- [56] Atsushi Togo, Fumiya Oba, Isao Tanaka, Phys. Rev. B 78 (2008) 134106.
- [57] G.K.H. Madsen, D.J. Singh, Comput. Phys. Commun. 67 (2006) 175.
- [58] T.J. Scheidemantel, C. Ambrosch-Draxl, T. Thonhauser, J.V. Badding, J.O. Sofo, Phys. Rev. B 68 (2003) 125210.
- [59] L. Jodin, J. Tobola, P. Pecheur, H. Scherrer, S. Kaprzyk, Phys. Rev. B 70 (2004) 184207.
- [60] L. Chaput, P. Pecheur, J. Tobola, H. Scherrer, Phys. Rev. B 72 (2005), 085126.
- [61] Atsushi Togo, Laurent Chaput, Isao Tanaka, Phys. Rev. B 91 (2015), 094306.
- [62] Li-Juan Wu, Yu-Qing Zhao, Chang-Wen Chen, Lin-Zhi Wang, Biao liu and meng-qi cai, Chin. Phys. B 25 (10) (2016) 107202.
- [63] W. Voigt, Lehrbuch der Kristallphysik: mit Ausschluss der Kristalloptik, B.G. Teubners Sammlung von Lehrbüchern auf dem Gebiete der mathematischen Wissenschaften mit Einschluss ihrer Anwendungen, J.W. Edwards, Ann Arbor, MI, 1928.
- [64] A. Reuss, Z. Angew. Math. Mech. 9 (1929) 49.
- [65] R. Hill, Proc. Phys. Soc. 65 (1965) 349.
- [66] Ibrahim Omer A. Ali, Daniel P. Joubert, Mohammed S.H. Suleiman, Eur. Phys. J. B 91 (2018) 263.
- [67] J. Feng, Apl. Mater. 2 (2014), 081801.
- [68] X. Luo, B. Wang, Structural and elastic properties of LaAlO₃ from first-principles calculations, J. Appl. Phys. 104 (7) (2008), 073518-24.
- [69] C. Li, Z. Wang, Computational Modelling and Ab Initio Calculations in MAX Phases – I. Advances in Science and Technology of Mn+1AX_n Phases, 2012, pp. 197–222.
- [70] G.P. Srivastava, Physics of Phonons, CRC Press, New York, 1990.
- [71] Gang Liu, Hong Yi Sun, Jian Zhou, Qing Fang Li, Xian-Gang Wan, New J. Phys. 18 (2016), 033017.
- [72] D.G. Cahill, S.K. Watson, R.O. Pohl, Phys. Rev. B 46 (1992) 6131.
- [73] Li Wu, Jesjs Carrete, K. Georg, H. Madsen, Natalio Mingo, Phys. Rev. B 93 (2016) 205203.
- [74] J. Freedman, J. Leach, E. Preble, et al., Universal phonon mean free path spectra in crystalline semiconductors at high temperature, Sci. Rep. 3 (2013) 2963.
- [75] Shuai Jing, Jun Mao, Shaowei Song, Qing Zhu, Jifeng Sun, Yumei Wang, Ran He, Jiawei Zhou, Gang Chen, J. David, Singh and zhifeng ren, Energy Environ. Sci. 10 (2017) 799–807.
- [76] David Parker, David J. Singh, J. Appl. Phys. 108 (2010), 083712.
- [77] Florian Huewe, Steefger Alexander, Kalina Kostoa, Laurence Burroughs, Irene Bauer, Strohriegl Peter, Vladimir Dimitrov, Simon Woodward, Jens Pflaum, Adv. Mater. (2017) 1605682.